Edge-state dynamics in coupled topological chains

M. Kurzyna and T. Kwapiński*
Department of Physics, Maria Curie Skłodowska University, 20-031 Lublin, Poland

(Received 30 June 2020; accepted 3 November 2020; published 23 November 2020)

We study time-dependent electrical properties of the Su-Schrieffer-Heeger (SSH) chain and coupled SSH chains on a substrate. Focusing on the midgap edge state dynamics we consider the abrupt transition from the normal to the SSH chain and determine characteristic timescale needed for topological states to develop. We have found that the midgap state is formed from the inside peaks of the normal chain density of states. For a ladderlike system we show that the edge SSH state vanishes in time or oscillates between neighboring sites. Moreover, for nonadiabatical time-dependent perturbations the midgap state can partially leak to other sites leading to induced topological states inside the trivial chain. We also analyze the mean-field correlation effects between the coupled chains revealing the induced Friedel oscillations in nontrivial chains.

DOI: 10.1103/PhysRevB.102.195429

I. INTRODUCTION

Science and engineering in past decades revealed a tendency of making things smaller and smaller. Quantum wires and atomic ribbons are the thinnest possible electric conductors [1–4] and they comprise basic blocks in nanoelectronics. Such low-dimensional systems reveal also many interesting quantum effects, such as conductance oscillations [5,6], spin-charge separation [7], charge-density waves [8], Majorana topological states [9,10], and others.

The study of topological quantum matter is one of the most attractive topic in low-dimensional physics. A Su-Schrieffer-Heeger (SSH) model is a simple tight-binding model in describing band topology in one-dimensional condensed-matter systems [11–17]. The SSH model has time-reversal, particle-hole symmetry, and it supports two distinct topological phases. The manifestation of the topological nontrivial nature in SSH systems is spectrally isolated midgap states localized at the system boundaries. These states are visible in the system density of states (DOS) and they are robust against local perturbations since they are related to the bulk environment (in contrast to conventional defect states which are sensitive to perturbations) [18]. Additional topological physics appear in extended SSH chains with more than two-site periodicity (larger unit cells) [19,20]. For long-range SSH models the site-site tunnelings include also next-nearest-neighbor hoppings or others couplings [11,21–24]. By expanding the standard SSH chain to a double-chain structure in a magnetic field one obtains the Creutz ladder model (cross-linked two-leg ladder system) or modified Harper model [25–27]. In ladderlike systems it is also possible to observe topological Majorana states [28]. Further expansion of a ladder leads to the ribbon SSH geometry or to strictly two-dimensional topological structures [29,30]. In contrast to equilibrium systems topological phases can be also induced by time-dependent external fields, e.g., the Floquet topological insulators [14,31–34]. Also a laser impulse applied to the SSH chain can generate high harmonics which depend on the system topological phase [35]. Moreover coherent destruction of tunneling in one-dimensional (1D) systems can appear as well [31,36,37].

There are a few experimental realizations of 1D topological systems. Very promising materials are stable atomic chains or atomic ribbons which can be grown epitaxially on reconstructed silicon surfaces, such as Si(335), Si(557), or others [1–4]. In such systems the scanning tunneling microscope (STM) measurement of the current-voltage characteristics or the conductance allows one to obtain the local density of states (LDOS) and distinguish different topological phases [38]. Additionally, with state-of-the-art fabrication technology it is possible to prepare 1D chains with gate-defined quantum dot (QD) in two-dimensional electron gas or chains of dopant atoms in silicon with STM [39,40]. In optics, the emerging field of topological photonics aims to fundamentally explore dynamical effects in 1D topological systems [41,42]. Using a photonic realization of the SSH chain it is possible to observe midgap nontrivial states of the SSH chain. Also, the extended SSH model with four-site periodicity were realized in a momentum lattice with ultracold Rb atoms [19]. In such systems topological properties can be estimated from the quench dynamics. Moreover, the Creutz ladder was realized in a driven 1D optical lattice on ultracold fermionic atoms [25]. This technique allows for arbitrary dynamical control over the tunneling phases, tunneling amplitudes or on-site energies [41,43]. Note that also 1D mechanical systems can manifest topological SSH properties [44,45] where the unit cell stands for two acoustic resonates or micromechanical junctions.

Electron transport properties of topological chains have been so far explored mainly in equilibrium (static) cases. Since new experimental techniques allow us to investigate atomic chains under time-dependent perturbations it would be desirable to obtain their time response on quenches and other perturbations. Thus far, such studies have been mostly

*tomasz.kwapinski@umcs.pl

focused on time- or space-dependent probability density of the boundary modes [46–48], whereas the energy-dependent spectral density dynamics of the edge states has been often overlooked. The time evolution of such functions gives deeper insight into the whole on-site energetic structure showing dynamical transitions between the bulk and the topological states. LDOS peaks can be interpreted as the system quasiparticle states and their behavior in time and energy domains is crucial for comprehensive studies of these systems. Similarly, dynamical phenomena of the coupled chains in different topological phases can be analyzed by the spectral density functions at both chains as they contain information about the edge states, gap structure, and normal (bulk) states evolution simultaneously. In this paper we consider such topological hybrid structures and, in particular, we would like to answer the questions: How fast does the edge state respond to an instantaneous or continuously changed perturbations? How is it built or destroyed in time? Moreover, it is desirable to analyze how fast such states could leak/penetrate into nontopological subsystems. In our studies we precisely address these questions and we concentrate on the spectral density function of the SSH chain and analyze its modifications due to the abrupt or adiabatical change in the topological phase. This process takes place when the nearest-neighbor couplings between sites change in time leading to transformation from the normal chain (characterized by uniform couplings) to the topological SSH chain (characterized by different intracell and intercell couplings). For a single atomic chain also other modifications of the couplings are studied, such as the transient effects after breaking the chain where suddenly new edge states appear in the energy gap region. We address the timescale typical for development of the edge states in topological chains. Moreover, we consider different combinations of coupled atomic chains including normal chain—SSH chain or two coupled SSH chains in different topological phases. For the double-chain structures we investigate evolution in time of the edge topological state between both chains and electron occupancy dynamics due to the Coulomb repulsion. Analytic results for such complex systems are hardly available but for some simplifications they are discussed in the paper.

As we are able to analyze full time dynamics of the spectral density function we have shown in the paper that topological edge states are formed directly from the inside peaks of the normal chain DOS and the timescale of this process strongly depends on the surface underneath the chain (which is discussed in Figs. 2–4). More importantly, time dynamics for the coupled chains of the same topological phases shows that the system energy gap is always closed for awhile after the quench (cf. Fig. 6), however, for the hybrid two-chain system composed of different phases the zero-energy state partially leaks to the nontrivial phase and it exists simultaneously at two different sites of this system (Fig. 10). It should be also emphasized the importance of the results discussed in Fig. 11 of this paper. We have found that in the presence of the Coulomb repulsion between both chains the induced Friedel oscillations in the SSH chain can be observed.

The paper is organized as follows. In Sec. II, we describe the theoretical model and the calculation method. In Sec. III, the main results of the paper are discussed for a single SSH chain on a substrate (Sec. III A), coupled chains in different topological phases (Sec. III B), SSH ladderlike chains in the presence of the Coulomb interactions (Sec. III C). Section IV gives a short summary.

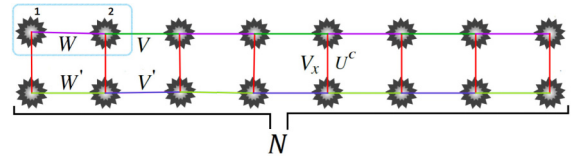

FIG. 1. Model of two coupled atomic chains of the length N that can be in different topological phases with the couplings W, V and W', V', respectively. V_x is the chain-chain coupling, and U^C stands for the Coulomb repulsion between charged sites.

II. MODEL AND THEORETICAL DESCRIPTION

The physical model we consider in this paper consists of a single atomic chain or coupled chains at the substrate as is schematically shown in Fig. 1. Each chain is composed of N single-electron sites with the nearest-neighbor couplings, W, V, W', V', V_x, and the Coulomb interaction U^C (repulsion). All parameters can change in time. The couplings along both chains can by uniform (as in the normal regular chain) or can vary periodically inside and between the primitive cell as in the SSH chain. For intracell couplings greater than intercell couplings we get a topological chain in the nontrivial phase, i.e., with topological midgap states at both chain ends (called here SSH_1), otherwise we obtain a chain in the trivial topological phase without end states (SSH_0).

The Hamiltonian of the system depends of the chain geometry and, in general, it can be written in the following form:

$$H = \sum_{i=1}^{M} \varepsilon_i a_i^\dagger a_i + \sum_{i=1}^{M} \sum_{\vec{k}_i} \left(\varepsilon_{\vec{k}_i} a_{\vec{k}_i}^\dagger a_{\vec{k}_i} + V_{\vec{k}_i,i} a_{k_i}^\dagger a_i + \mathrm{H.c.} \right) + \sum_{i,j}^{M} V_{i,j}(t) a_i^\dagger a_j + \sum_{i,j}^{M} U_{i,j}^C(t) \hat{n}_i \hat{n}_j, \quad (1)$$

where M is the total number of sites in the system, $a^\dagger$, a are the creation and annihilation electron operators at the appropriate sites, $\hat{n}_i = a_i^\dagger a_i$ is the particle number operator, ε_i and $\varepsilon_{\vec{k}}$ stand for the single-electron energies in the chain or in the substrate, respectively (the substrate is considered as M-separate electrodes). Electron transitions between the surface and the sites are established by the couplings $V_{\vec{k},i}$ and $V_{i,j}$ correspond to the nearest-neighbor tunneling between the chain sites (the coupling between chains corresponds to $V_{i,j} = V_x$ and is site independent). The last term in the Hamiltonian $U_{i,j}^C \hat{n}_i \hat{n}_j$ stands for the site-site Coulomb repulsion, and it is assumed that this interaction is captured within the mean-field (Hartree-Fock) approximation which renormalizes the single-electron energies in the Hamiltonian, i.e., $\varepsilon_i \to \varepsilon_i + U_{i,j}^C n_j$, where n_j is the expectation value of $\hat{n}_j$. This approach is justified as the Coulomb interaction in many quantum structures is small [such as in Pb chains on the Si(335) surface], thus, noninteracting eigenstates of the quantum structure are related to those of small U^C. In the opposite limit (large U^C) the energetic structure of the system is split with the Coulomb blockade

gap, but if we neglect many-body complex effects, such as the Kondo effect, it is reasonable to focus on a single Coulomb band. Thus, the spin index in our calculations is suppressed as both spin directions are independent.

In order to describe time response of the system on external perturbations the evolution operator method is used in our calculations [49,50]. The charge occupation of the ith site can be expressed in terms of the appropriate matrix elements of the evolution operator (for details see Appendix A),

$$n_i(t) = \sum_{j=1}^{M} n_j(t_0)|U_{i,j}(t,t_0)|^2 + \sum_{j,\vec{k}_j} n_{\vec{k}_j}(t_0)|U_{i,\vec{k}_j}(t,t_0)|^2, \qquad (2)$$

and the current flowing from the surface electrode is obtained from the time derivative of the total number of electrons in this reservoir,

$$j_1(t) = -e\frac{d}{dt}N_1(t) = -e\frac{d}{dt}\sum_{\vec{k}_1} n_{\vec{k}_1}(t), \qquad (3)$$

where $n_{\vec{k}_1}(t)$ is expressed similarly to Eq. (2) and $n_\alpha(t_0)$ is the initial occupancy of state α. In the interaction representation the evolution operator matrix elements satisfy the following equation of motion:

$$i\frac{\partial}{\partial t}U(t,t_0) = \hat{V}(t)U(t,t_0), \qquad (4)$$

where $\hat{V}(t) = U_0(t,t_0)V(t)U_0^\dagger(t,t_0)$, $U_0(t,t_0) = \mathcal{T}\exp\left(i\int_{t_0}^{t} dt' H_0(t')\right)$ and $\mathcal{T}$ is the time-ordering operator. Here $V(t)$ and $H_0(t)$ are the coupling part and the on-site energy part of the total Hamiltonian, respectively ($H_0 = \sum_\alpha \varepsilon_\alpha a_\alpha^\dagger a_\alpha$). In the calculations we put the initial time $t_0 = 0$ (i.e., the couplings are zero for $t < t_0$), and all dynamical effects are analyzed for the system which already reaches its equilibrium state so the initial occupations of the chain sites do not play any role, thus, we assume $n_i(t_0) = 0$. In such a case the chain occupancies can be written as $n_i(t) = \sum_{j,\vec{k}_j} n_{\vec{k}_j}(0)|U_{i,\vec{k}_j}(t)|^2$. The summation over the wave vectors with the initial band fillings $n_{\vec{k}_j}(0)$ is, as usual, replaced by the integral over the energy with the Fermi function $f(\varepsilon)$, i.e., $n_i(t) = \int d\varepsilon \sum_j f(\varepsilon)D_j(\varepsilon)|U_{i,\vec{k}_j}(t)|^2 = \int d\varepsilon\, f(\varepsilon)\mathrm{LDOS}_i(\varepsilon,t)$, where $D_j(\varepsilon)$ is the jth electrode bandwidth and $\mathrm{LDOS}_i(\varepsilon,t)$ is the spectral density function (the local DOS) at the ith site. The evolution operator $U_{i,\vec{k}_j}(t)$ can be found from Eq. (4), and after some algebra (see Appendix A) the differential equation on this function takes the form

$$\begin{aligned} i\frac{\partial U_{i,\vec{k}_j}(t)}{\partial t} = &\sum_{i'} V_{ii'}e^{i(\varepsilon_{i'}-\varepsilon_i)t}\exp\left[iU^C\int_0^t dt'\widetilde{n}_{i'}(t') - \widetilde{n}_i(t')\right]U_{i',\vec{k}_j}(t) \\ &- V_{i\vec{k}_j}e^{i(\varepsilon_i-\varepsilon_{\vec{k}_j})t}\exp\left[iU^C\int_0^t dt'\widetilde{n}_i(t')\right] \\ &- |V_{i\vec{k}_j}|^2\int_0^t dt' D(t-t')e^{i\varepsilon_i(t-t')}\exp\left[iU^C\int_{t'}^t dt_1\widetilde{n}_i(t_1)\right]U_{i,\vec{k}_j}(t'), \end{aligned} \qquad (5)$$

where $\widetilde{n}_i(t) = \sum_{j'} n_{j'}$ and j' runs over all neighboring sites (from the ith site) for which there is U^C repulsion between electrons, $U_{ij}^C = U^C$. The time-dependent current, Eq. (3), is also expressed by means of the evolution operator matrix elements, see Eq. (A5), and can be written as follows ($e = 1$):

$$\begin{aligned} j_1(t) = -2\,\mathrm{Im}&\left\{\sum_{\vec{k}_1} n_{\vec{k}_1}(0)V_{\vec{k}_1}e^{i(\varepsilon_{\vec{k}_1}-\varepsilon_1)t}\exp\left[-iU^C\int_0^t dt'\widetilde{n}_i(t')\right]U_{1,\vec{k}_1}(t)\right\} - 2\,\mathrm{Re}\left\{\sum_{\vec{k}_i} n_{\vec{k}_i}(0)|V_{\vec{k}_1}|^2U_{1,\vec{k}_i}(t)\right. \\ &\left.\times\int_0^t dt' D_1^*(t-t')e^{i\varepsilon_i(t'-t)}\exp\left[iU^C\int_{t'}^t dt_1\widetilde{n}_i(t_1)\right]U_{1,\vec{k}_i}^*(t')\right\}, \end{aligned} \qquad (6)$$

where $D(t) = \int d\varepsilon\, D(\varepsilon)e^{i\varepsilon t}$ is the time Fourier transform of the lead DOS, $D(\varepsilon)$. Note that the knowledge of $U_{i,\vec{k}_j}(t)$ is necessary to obtain the chain occupancies, spectral density function, or the currents. In general, analytical expressions for these quantities do not exist, and the problem should be resolved numerically. However, some analytical solutions are possible in the wideband approximation as well as for regular and symmetrical chains which will be discussed later in the paper. Assuming the wideband approximation, the influence of the substrate can be captured by the site-dependent spectral density Γ_{ij}, which diagonal elements play the crucial role and are energy independent: $\Gamma_{ii}(\varepsilon) = 2\pi\sum_{\vec{k}}|V_{i\vec{k}}|^2\delta(\varepsilon-\varepsilon_{\vec{k}}) = \Gamma_i$. The off-diagonal terms rapidly vanish with the site-site distance and in the paper are negligible, thus, the surface electrode can be considered as a set of equivalent leads such that each chain site is coupled with its own electrode Γ_i. Within this approach one can obtain the time integral in the last term in Eq. (5) which equals $i\frac{\Gamma_i}{2}U_{i,\vec{k}_j}(t)$. In this case the relation for the current, Eq. (6), can be written as follows:

$$j_1(t) = -2\,\mathrm{Im}\left\{\sum_{\vec{k}_1} n_{\vec{k}_1}(0)V_{\vec{k}_1}e^{i(\varepsilon_{\vec{k}_1}-\varepsilon_1)t}\exp\left[-iU^C\int_0^t dt'\widetilde{n}_i(t')\right]U_{1,\vec{k}_1}(t)\right\} - \Gamma_1 n_1(t). \qquad (7)$$

Note that similar equations for other currents $j_i(t)$ can be derived which should be resolved using the set of differential equations, Eq. (5), together with the relations for $n_i(t)$.

III. RESULTS AND DISCUSSION

Here we analyze electron transport properties of a single chain and coupled atomic chains on a surface focusing on the time evolution of the occupancies, spectral density functions (LDOS), or the currents for different chain geometry. We carry out the quench to the system by suddenly or adiabatically changing some hopping parameters. In our calculations we assume the temperature $T = 0$ K, and the energy reference point stands for the Fermi energy of the surface electrode, which implies $E_F = 0$. Moreover, equal on-site energies for all sites are considered $\varepsilon_i = \varepsilon_0$, and the parameters are chosen to fit the realistic parameters measured in experiments. In our calculations we use the effective chain-lead coupling $\Gamma_i = \Gamma$ as the energy unit, then for $\Gamma = 0.1$ eV, the coupling $V = 4$ corresponds to $V = 0.4$ eV, the time unit is $\hbar/\Gamma \simeq 10^{-15}$ s, and the current unit becomes $2e\Gamma/\hbar \simeq 50\ \mu$A.

A. Single atomic chain

We start by addressing the time-evolution effect of the normal atomic chain which evolves (is transformed) to the topological one and consider a linear chain on a surface for which some analytical expressions can be derived for the uncorrelated case $U^C = 0$. The transition from the normal to topological chain is forced by changing in time the hopping integrals inside the chain.

For a finite 1D system composed of N equal sites in the stationary case one can obtain analytical results, e.g., for the conductance [51]. The Hamiltonian of the SSH chain has chiral symmetry which gives rise to a symmetric energy spectrum and for periodic boundary conditions the results can be also derived analytically [17]. The situation is more complicated for time-dependent transport properties, especially for a chain on a noninsulating substrate. To calculate the time-dependent on-site spectral density function one needs $U_{i,\vec{k}_j}(t)$ matrix elements which can be found using the Laplace transform technique (see Appendix B). After some algebra we find the solution, e.g., for $U_{1,\vec{k}_j}(t)$, which is necessary in the spectral density function $\mathrm{LDOS}_1(\varepsilon)$,

$$U_{1,\vec{k}_j}(t) = \frac{(-i)^j V^{j-1} V_{j,\vec{k}_j} \prod_{j_1=1}^{N-j} \left(s_0 + \frac{\Gamma}{2} + 2iV\ \cos\frac{j_1\pi}{N-j+1} \right)}{\prod_{j_1=1}^{N} \left(s_0 + \frac{\Gamma}{2} + 2iV\ \cos\frac{j_1\pi}{N+1} \right)} \exp\left(i(\varepsilon_0 - \varepsilon_{\vec{k}_j})t\right)$$
$$+ \sum_{j_1=1}^{N} \frac{(-i)^j V^{j-1} V_{j,\vec{k}_j} \prod_{j_2=1}^{N-j} \left(s_{j_1} + \frac{\Gamma}{2} + 2iV \cos\frac{j_2\pi}{N-j+1} \right)}{[s_{j_1} - i(\varepsilon_0 - \varepsilon_{\vec{k}j})] \prod_{j_2=1,\, j_2\neq j_1}^{N} \left(s_{j_1} + \frac{\Gamma}{2} + 2iV\ \cos\frac{j_2\pi}{N+1} \right)} \exp\left(-\frac{\Gamma}{2}t\right) \exp\left(-2\,iV \cos\frac{j_1\pi}{N+1}t\right), \quad (8)$$

where $s_0 = i(\varepsilon_0 - \varepsilon_{\vec{k}j})$ and $s_j = -\frac{\Gamma}{2} - 2iV\ \cos\frac{j\pi}{N+1}$. Note that the above function oscillates in time (even far from the initial time t_0) and is responsible for time dynamics of the system. The spectral density function is expressed by $|U_{1,\vec{k}_j}(t)|^2$ elements, which also oscillates in time, but for large t (far from the perturbation) it reads

$$|U_{1,\vec{k}_j}(t \to \infty)|^2 = \frac{V^{2(j-1)} V_{j,\vec{k}_j}^2 \prod_{j_1=1}^{N-j} \left[\left(\varepsilon_0 - \varepsilon_{\vec{k}_j} + 2V\ \cos\frac{j_1\pi}{N-j+1} \right)^2 + \left(\frac{\Gamma}{2}\right)^2 \right]}{\prod_{j_1=1}^{N} \left[\left(\varepsilon_0 - \varepsilon_{k_j} + 2V\ \cos\frac{j_1\pi}{N+1} \right)^2 + \left(\frac{\Gamma}{2}\right)^2 \right]}, \quad (9)$$

and is time independent. There are N product terms in the denominator of the above relation, which minima determine the spectral density peaks. Note that analytical formulas for the current or site occupancies are possible in this case, but they do not have short transparent form.

To study the time-response effects in our calculations we use Eq. (8) for $U_{i,\vec{k}_j}(t)$ (for regular chains) or resolve numerically the set of differential equations Eq. (5) for arbitrary time-dependent chains. In the beginning we analyze in Fig. 2 the transition effect form the normal chain (described by uniform couplings) to the topological one in the nontrivial phase (SSH_1) for the chain length $N = 8$ placed on the surface. The left, middle, and right panels show the time evolution of the spectral density function at the first, second, and third chain sites, respectively, and the transition takes place at $t = 20$ (i.e., far from the transient effects observed for the initial time). Before this time the chain spectral density is fixed (does not change in time) and for $i = 1$ is expressed by Eq. (9). It is expected that at this site, just after the quench, the energy gap should be opened and simultaneously the midgap state

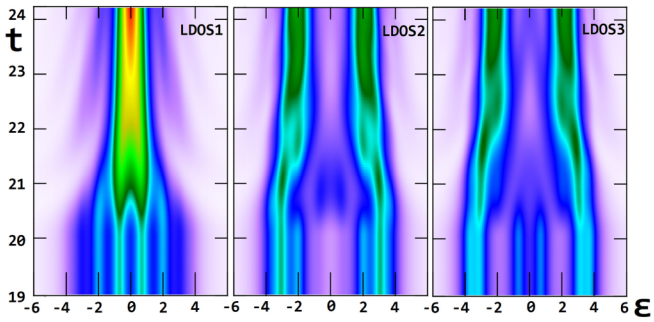

FIG. 2. LDOS time evolution of the normal chain ($V = W = 2$) composed of $N = 8$ sites on the surface for sudden change of the couplings to the SSH parametrization in the nontrivial phase ($W = 0.5$, $V = 2.0$) at $t = 20$. Other parameters are $\varepsilon_0 = 0$, $\Gamma_i = \Gamma = 1$, $U^C = 0$. Red, yellow, green, and blue colors represent the LDOS values equal to 0.6, 0.4, 0.2, and 0.1, respectively.

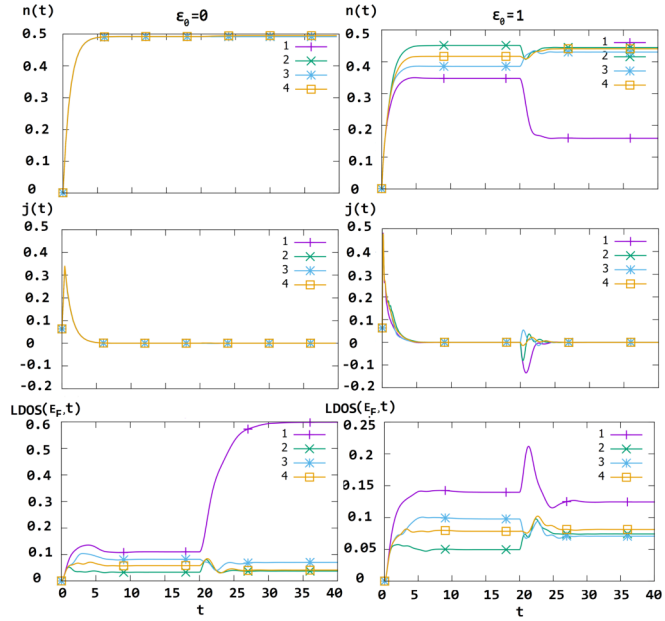

FIG. 3. Time-dependent charge occupancies, currents, and LDOS at the Fermi level (upper, middle, and bottom panels, respectively) for first four sites of the normal chain of length $N = 8$ ($V = W = 2$) switched at $t = 20$ to the SSH_1 nontrivial chain with the couplings $W = 0.5$, $V = 2.0$ for different on-site energies $\varepsilon_0 = 0$ (left panels) and $\varepsilon_0 = 1$ (right panels).

should appear. We would like to analyze how this edge state is formed in time: Is it built directly from the normal states, or do these states disappear and then the midgap state arises? To answer this question we have to consider the full time- and space-dependent LDOS because the occupation number or topological invariants cannot resolve this problem. As one can see at $t = 20$ the LDOS at each site is rebuilt in time and the energy gap of the width $\pm 2\eta$ appears along the chain with the midgap topological states at both chain ends (in our case we have $W = 1.25 - \eta$ and $V = 1.25 + \eta$ with $\eta = 0.75$). A careful inspection on the time evolution of LDOS shows that the topological state does not appear just after the quench but it needs few time units to be fixed (about ten time units). More important, during this process the states evolve continuously (without delocalization), and in the first stage the midgap state is built from the central DOS peaks of the normal chain (two peaks join together just after $t = 20$). At the same time two next peaks localized at $\varepsilon = \pm 2$ are bent towards the zero energy (band center) and after some next period of time they reach our topological state. The energy-dependent spectral functions of the interchain sites are characterized by two main sidebands (greenlike regions, Fig. 2, middle and right panels for $t > 20$) with the energy gap between them. However, in contrast to the topological state these bands are formed in a different way: The central LDOS peaks of the normal chain (around the Fermi level) do not support these sidebands, but they vanish very fast after the quench (better visible in the right panel) and the sidebands are smoothly built only from the most outer LDOS peaks.

To study this dynamical process in more detail in Fig. 3 we analyze the charge occupation, currents, and LDOS at the Fermi energy for the first four sites of the system for the same parameters as in Fig. 2. We also compare dynamics of the system for two different values of the on-site energies $\varepsilon_0 = 0$ (symmetrical case) and $\varepsilon_0 = 1$ (asymmetrical case). The transient (turn-on) effects appear in the system only for very small t such that for $t > 10$ the system is in the equilibrium state. For the symmetrical case all sites are half-occupied (upper left panel), and they are almost unaffected by the quench at $t = 20$. It results from the fact that stationary occupancies n_i for the normal and topological chains are exactly the same for $\varepsilon_0 = 0$, and the spectral density changes symmetrically in time for positive and negative energies (as is shown in Fig. 2). It leads to constant occupancies in the chain during the transition. However, even for constant $n_i(t)$, the charge could flow through the system, thus, it is necessary to analyze the electron currents [obtained from Eq. (7)]. It turns out that beyond the initial time the currents do not flow from the substrate to the chain (middle left panel) which confirms that electron charges are localized along the chain and do not flow during the transition. In the bottom panels of Fig. 3 we analyze the spectral density function at the Fermi level. As one can see the LDOS at the first site (with the midgap topological state) grows monotonically just after the quench whereas other middle-chain sites reveal small vanishing in time oscillations. However, the spectral density $LDOS_1$ does not change smoothly but reveals some inflection points which are related to the creation process of the midgap state discussed in Fig. 2. One can note that the spectral density at the first site needs much longer time to reach its equilibrium value (ten units) than the LDOS at other sites. The studies of the reverse process (quench from nontrivial to the trivial phase) leads to very similar results with monotonically decreasing value of the local DOS at the edge sites. However, the midgap state changes just after the quench and is not frozen, cf. Ref. [48] due to the chain-surface coupling which is responsible for the rate of the transition.

For the non-symmetrical case ($\varepsilon_0 \neq E_F$, right panels) the physics of the chain transition is much reacher. Now the occupancies along the normal chain (i.e. before the quench) form a kind of charge waves in the system [8,52]. Next, for

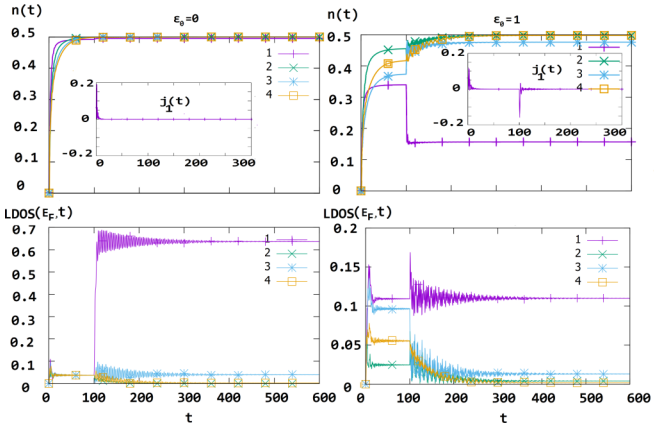

FIG. 4. Electron occupancies (upper panels) and LDOS at the Fermi level (bottom panels) of the first four sites in the normal chain ($V = W = 2$) switched to the nontrivial topological chain ($W = 0.5,\ V = 2.0$) at $t = 100$ for $N = 8,\ \Gamma_1 = \Gamma_N = 1,\ \Gamma_i = 0$ for $\varepsilon_0 = 0$ (left panels) and $\varepsilon_0 = 1$ (right panels). The insets in the upper panels show the left current $j_1(t)$.

$t > 20$ the chain couplings are changed and the occupancies at the middle-chain sites tend to some constant value, common for all sites (almost half-occupied) because the energy gap appears along the chain and the Fermi energy is still in this energy gap region ($\varepsilon_0 = 1,\ E_F = 0$ and the energy gap width is 3). However, the occupancy of the end site rapidly decreases after the quench as now the midgap state is shifted towards ε_0 and there is a relatively low value of LDOS at the Fermi level. The consequence of this asymmetry in the LDOS is the current flowing from the substrate to the chain (middle right panel). The largest quench current appears for the first site because its occupancy rapidly decreases and the excess charge flows out to the surface (the current is negative). Note that other currents $j_i(t)$ oscillate in time and can be positive or negative depending on the occupancy modifications at a given site. All currents flow only for a short period of time after the quench (few time units) and then the system tends to its equilibrium state, thus, the currents vanish. Also the spectral functions at the Fermi level (right bottom panel) show damping oscillations after the quench and tend to the same asymptotic values for all middle sites and to the higher value of the LDOS at the edge site (due to the midgap state).

The transition from the normal to the topological system changes the structure of LDOS along the chain, but the system reaches its steady state relatively fast (almost monotonically or with small damping oscillations). For the chain on a substrate each site is coupled with continuum states in the lead underneath, and the oscillations are strongly suppressed. However, it could be interesting to study the transition effect for a chain on the insulating substrate. Thus, we consider the chain in the L-R geometry, i.e., the chain is coupled only with two (left and right) external electrodes via the edge sites ($\Gamma_1 = \Gamma_N = 1$ and $\Gamma_i = 0$). The results for symmetrical ($\varepsilon_0 = 0$) and nonsymmetrical ($\varepsilon_0 = 1$) spectral density functions are shown in Fig. 4, left and right panels, respectively, and the transition takes place at $t = 100$. In this case the system needs much more time to go beyond the transient effects—the sites are charged up to $t \simeq 80$ (upper panels) whereas for the noninsulating surface this time was ten times smaller. Now lead electrons have to pass through all chain sites to occupy the middle sites. As before, for the symmetrical case the occupancies do not change during the transition and the current does not flow in the system (left upper panel). However, for the nonsymmetrical case the occupancies change their values after the quench (right upper panel) especially at the edge site and oscillate with small damping amplitudes. These oscillations are also visible on the spectral density functions at the Fermi level (bottom panels)—they vary in time with slowly damping oscillations for both symmetrical as well as nonsymmetrical cases. During these oscillations a new spectral density function is formed at each site similar to the noninsulating surface discussed in Fig. 2—the main difference is that for the insulating surface the spectral density does not change smoothly but it oscillates even for hundreds of time units after the quench with slowly vanishing amplitude. However, it is worth noting that the surface coupling Γ_i is responsible for the half-width of the LDOS peaks, thus, the asymptotic occupancies are almost not sensitive to this coupling strength. We have also considered different chain lengths N, and the results remain still valid. However, we have found that the LDOS oscillations can reveal quantum beats which are size dependent (not shown here). It turns out that these beats behave in the same way as the survival probability obtained for 1D Majorana modes [46].

Electrical properties of stationary atomic chains are well known, e.g., topological states of such systems are protected against external perturbations and survive when the chain is coupled with the substrate [18]. However, it is desirable to check if this protection is still present for time-dependent perturbations especially just after the quench. To study this effect we consider the SSH_1 chain with the midgap edge states and at a given time $t = 20$ suddenly break the chain into two smaller parts (the chain is broken between the eighth and the ninth sites). This situation is schematically shown in Fig. 5 (upper scheme). The relevant spectral density functions at four chosen sites are shown in the lower panels. One can observe that topological state at the first site is unchanged in time, thus, it is protected against such perturbations. We can also note that internal sites are slightly affected by this destructive process (middle and right panels in Fig. 5) and, e.g., even the last but one site from the perturbation ($LDOS_7$) remains almost unchanged for $t > 20$. Also the occupancies do not change in time in this case because all spectral density functions are symmetrical versus the Fermi energy. What is important, just after the breaking one observes time formation of the topological midgap states at the eighth (bottom panel) and ninth sites in the chain as these sites became new edges for two separated topological chains. These states are smoothly formed from the bulk sidebands of the topological chain. It is worth noting that in this case the perturbation is sharp but the states are not smashed over the energy scale (no decoherence effects) and the LDOS at new edge sites smoothly changes in time by bending the sidebands towards the Fermi energy.

B. Coupled atomic chains

Thus far, we have analyzed midgap state dynamics in a single atomic chain. However, in real systems such a chain

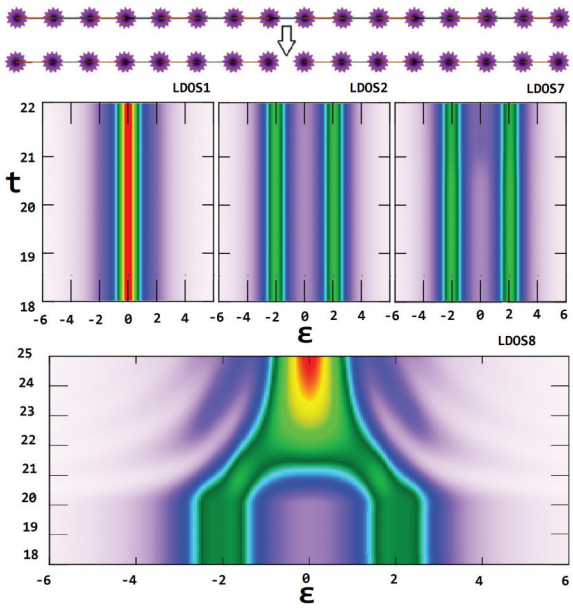

FIG. 5. LDOS time evolution at the first, second, seventh, and eighth sites for the nontrivial chain composed of $N = 16$ sites on the surface ($W = 0.5$, $V = 2.0$) broken at $t = 20$ between the eighth and the ninth sites as is indicated in the upper scheme $\varepsilon_0 = 0$, $\Gamma_i = 1$.

is fabricated in the vicinity of other regular chains, such as on vicinal surfaces Si(335) or Si(557) where two or more parallel chains can be observed at each terrace [1,4]. On the other hand coupled chains are more stable and perspective in nanoelectronics than a single atomic chain which can easily break. In real experiments the site-site hoppings can be modified by changing the distances between atoms (e.g., using the STM technique, varying the substrate temperature, using piezoelectric substrates, or in optical lattices). Alternatively, one can use a linear QD system where all couplings between dots can be fully controlled by external electrodes. Thus, it is desirable to investigate the electronic properties of coupled chains on a surface, in particular, to determine time dynamics of topological states in the presence of neighboring chains being in the same or other topological phase.

First, in Fig. 6 we consider two coupled chains in the same topological phases, i.e., SSH_0-SSH_0 or SSH_1-SSH_1. For such ladderlike systems we analyze the spectral density dynamics for two sites $LDOS_1$ and $LDOS_2$ (which are the same for both chains). The coupling V_x changes in time linearly (quenchlike changes) from zero (at $t = 10$) to $V_x = 10$ (at $t = 11$) and before the quench ($t < 10$) both chains are in their initial topological phases, i.e., the trivial phase with the energy gap along the whole chain (SSH_0) or in the nontrivial phase with the midgap edge states (SSH_1). It is interesting that for the SSH_0-SSH_0 system after the quench the sidebands of the LDOS observed for $t < 10$ split in time by the value $\pm V_x$ and they form four separated sidebands (indicated by the arrows). During this process the energy gap is closed for awhile as the sidebands cross together—see the bluelike horizontal stripes around $\varepsilon = 0$ for $t \simeq 10$. Note that for the small value of V_x the splitted sidebands do not cross each other and the energy gap is not closed in that case. This effect is confirmed by the

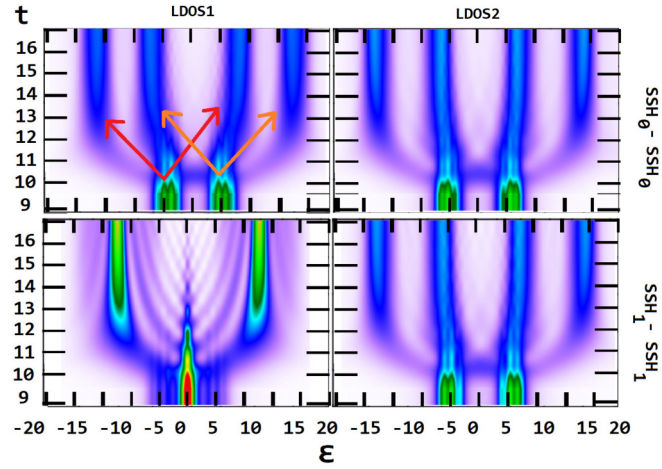

FIG. 6. LDOS time evolution of two first sites $LDOS_1$, $LDOS_2$ (left and right panels) for SSH_0-SSH_0 and SSH_1-SSH_1 coupled chains with $V = 2$, $W = 4$ (SSH_0) and $V = 4$, $W = 2$ (SSH_1). The coupling between chains is switched on linearly from zero (at $t = 10$) to $V_x = 10$ (at $t = 11$), $\Gamma_i = 1$, $\varepsilon_0 = 0$, $N = 10$.

energy spectra calculations shown in the upper panel in Fig. 7 for the SSH_0-SSH_0 system. The spectrum has a reflection symmetry through the Fermi energy in the gap due to the particle-hole symmetry. One can see that for small hopping V_x the energy gap still exists then it is closed for intermediate values of V_x and for larger hoppings it opens again. It is the reason that during the large jump of this parameter the system is not transformed immediately to the energy gap region, but

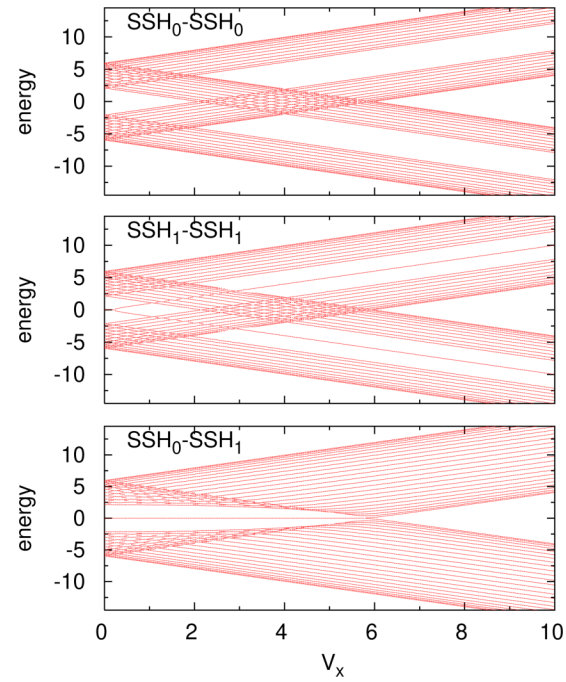

FIG. 7. Quasienergy spectra of two coupled atomic chains as a function of the chain-chain hopping V_x for two SSH_0 chains (upper panel), two SSH_1 chains (middle panel), and for SSH_0-SSH_1 chains of the length $N = 24$. The other parameters as the same as in Fig. 6.

for a moment the energy gap is closed. Note, however, that quasienergy spectra do not give us as wide perspective on the quantum states dynamics as the time- and space-dependent LDOS function. Similar behavior of the LDOS dynamics we observed for all sites in the SSH_0-SSH_0 system as well as for all intersites of the SSH_1-SSH_1 system (e.g., right bottom panel in Fig. 6). At these sites there are no topological states at the Fermi level—the energy spectrum for the SSH_1-SSH_1 geometry is shown in the middle panel in Fig. 7 and the gap existence for large V_x is evident. Note that there are also further gaps in the energy spectra beyond the Fermi level and for the nontrivial phase additional states in the middle of these gaps can exist [38]. The most interesting is the midgap topological state dynamics (left bottom panel in Fig. 6). Here the edge state slowly vanishes and reveals damping oscillations in the energy gap region. Moreover, only two main sidebands are formed at the edge site and these sidebands are accrued from the midgap state by "periodical emission" of the main state towards the sidebands. The emission process takes place when the midgap state reaches maximal values during its oscillations in time. It leads to a nice symmetrical picture with periodical spectral density oscillations in the energy gap region and this effect will be discussed later.

Next we consider two coupled chains that are in different topological phases. The system is composed of the SSH_1 (nontrivial phase) and SSH_0 (trivial phase) chains. In Fig. 8 we show the LDOS at the first two sites of the SSH_1 (left panels) and SSH_0 (right panels) topological chains which are coupled at $t = 10$. We consider different time rates of this coupling: It is switched on very slowly [adiabatically, panels (a)], average [panels (b)], and rapidly [fast quench, panels (c)] as is indicated in the upper inset. For adiabatically changed coupling V_x we observe the monotonically vanishing (without oscillations) topological state at the edge site of the nontrivial SSH_1 chain [left (a) panel], and for $t \simeq 55$, which corresponds to $V_x \simeq 6$, this state disappears. It is confirmed by the quasienergy spectrum for this system shown in Fig. 7, bottom panel, where the bulk energy gap of the SSH_0-SSH_1 system with the midgap state closes for $V_x \simeq 6$ and opens again without the appearance of any topological state for larger V_x. Thus, the system changes its topology from the nontrivial phase to the trivial one. Interestingly, that in the trivial chain at the second site, additional midgap state appears in the spectral density for the coupled chains. This state is visible only for a short period of time (which corresponds to $V_x < 6$), and for larger t it smoothly vanishes. The appearance of this induced state in the SSH_0 chain is correlated with the intensity of the edge state in the SSH_1 chain—one can say that the topological state leaks for a moment to the trivial chain. It is important that this process holds between nondirectly coupled sites in both chains and there is still an energy gap in their neighboring sites at the Fermi level [middle (a) panels]. To confirm this conclusion we analyze in more detail the LDOS at the Fermi energy as a function of time and in Fig. 9(a), one can see that the midgap topological state (purple curve) slowly vanishes for $t > 10$ and at the same time the induced state in the trivial chain appears (orange curve). For a longer time (larger V_x value) the energy gap closes (around $t = 50$) and opens again with the trivial phase without topological states.

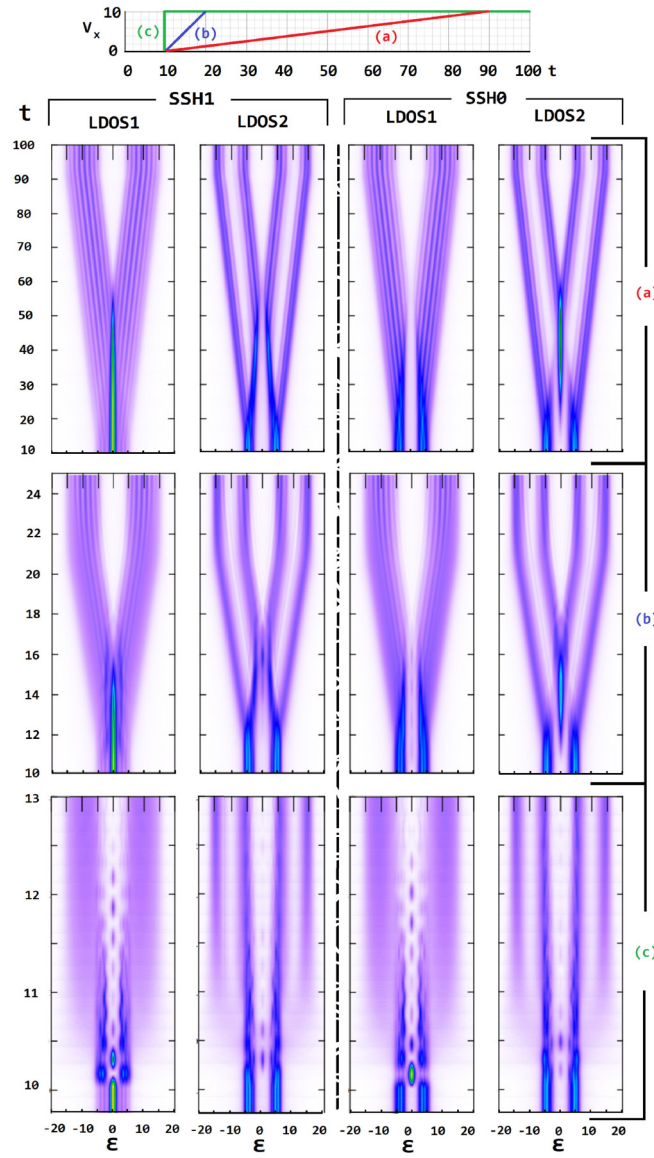

FIG. 8. Time evolution of the LDOS at two sites $i = 1, 2$ of initially decoupled chains of the length $N = 10$ in different topological phases (SSH_0 with $V = 2$, $W = 4$ and SSH_1 with $V = 4$, $W = 2$). The chains are coupled at $t = 10$ and $V_x(t)$ changes in time as is indicated in the upper inset according to the (a), (b), or (c) curve, respectively.

More interesting physics appears for nonadiabatical perturbations where the chain-chain hopping rapidly change in time [(b) and (c) panels in Fig. 8]. Topological edge states in the SSH_1 chain vanish with time [left (b) panel] and the midgap state in the trivial SSH_0 chain (at the second site) is observed during the fast linear change of V_x which is shown in the right (b) panel. For this change there is still a short period of time for which V_x corresponds to the nontrivial SSH phase and the induced topological state can appear for a moment. This dynamical process is also visible in Fig. 9, (b) panel where the spectral density functions at the Fermi level are shown for the first two sites of both chains. As before, the topological state vanishes in time (purple curve), but now small oscillations of LDOS are evident. Note that rate-dependent oscillations after

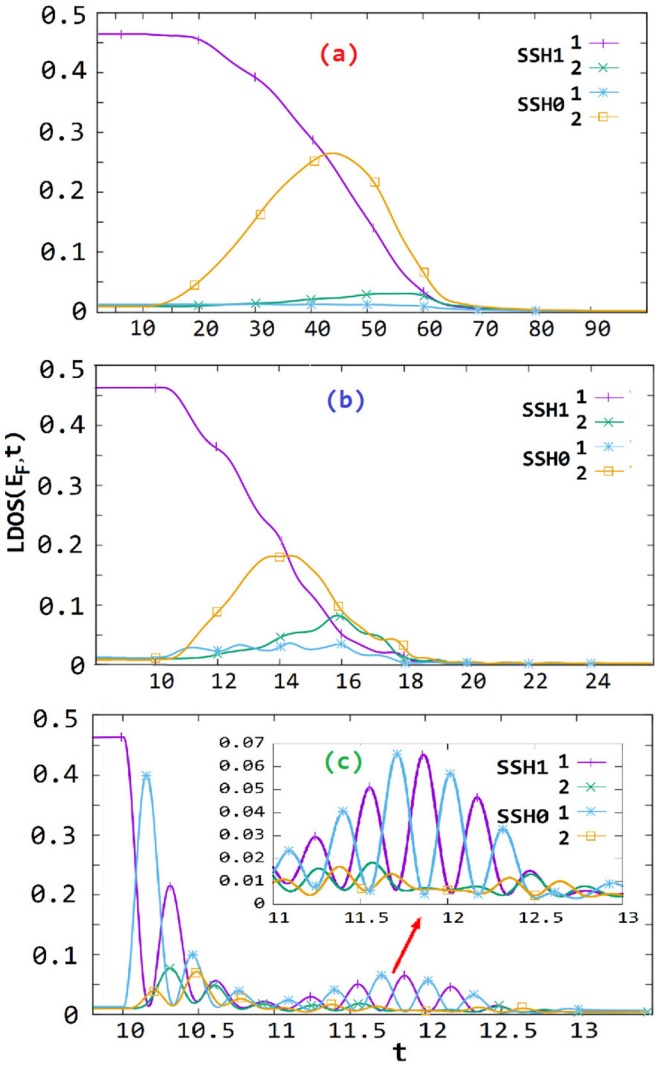

FIG. 9. LDOS at the Fermi energy at two sites ($i = 1$ and $i = 2$) for the same system as in Fig. 8: SSH_0-SSH_1 chains coupled together at $t = 10$ for different V_x changes (a), (b), and (c), respectively. All parameters are the same as in Fig. 8.

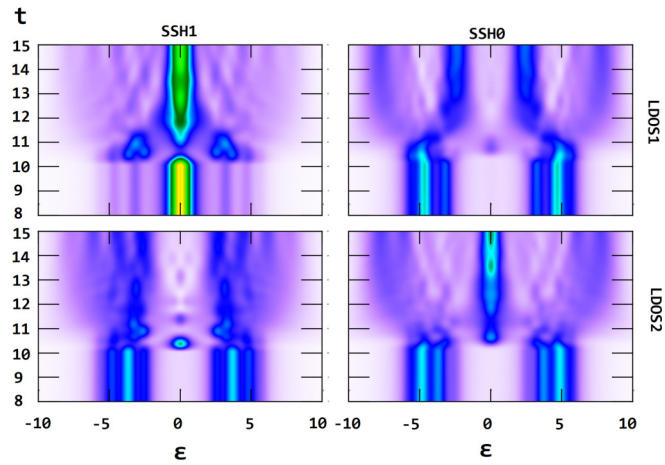

FIG. 10. Time evolution of the LDOS at $i = 1$ and $i = 2$ sites of atomic chains composed of $N = 8$ sites each being in different topological phases (SSH_0 and SSH_1). At $t = 10$ chains are immediately connected [similarly as in Fig. 8, (c)] $V_x = 3$ and all other parameters are the same as in Fig. 8. Yellow, green, and blue colors represent the LDOS values equal to 0.4, 0.2, and 0.1, respectively.

the quench were also observed for the Majorana probability mode where these oscillations increase as the rate of quench becomes larger [47] and for small rates these oscillations are hardly observed. Similarly, the induced midgap state in the SSH_0 chain appears for a moment with small oscillations. For larger t the energy gap is open again (trivial phase), and this induced state vanishes in time. Moreover, in this case the LDOS at the neighboring sites (in SSH_1—the second site, and in SSH_0—the first site) have small nonzero values after the quench and they also oscillate in time. It means that the SSH_1 topological state is now transferred also to the neighboring sites. However, for the abrupt change in V_x [sudden change from zero to a finite large value, panel (c) in Fig. 8] the system is transformed directly to the trivial phase and it never takes intermediate values of V_x. Thus, it is not obvious that the topological induced state could appear in the trivial chain during the quench. To answer this intriguing question we study this effect in the (c) panel and find that after the quench the system tends to the trivial phase [as was discussed in (a) and (b) panels], however, we observe that the midgap states appear for a short period of time at the Fermi level in both chains. These induced states do not vanish monotonically, but they reveal oscillations in time. The oscillations are strictly correlated with the vanishing topological state oscillations in the nontrivial SSH_1 chain and are analyzed in more details in Fig. 9, (c) panel. As one can see now the oscillations of LDOS(E_F) at the SSH_0 sites are in the same phase (blue and orange curves) and in the SSH_1 sites are in phase (purple and green curves). However, there are alternating (antiphase) oscillations between sites in both chains, thus, the maximal values of LDOS(E_F) at first SSH chain are correlated with minimal values of LDOS(E_F) at the second chain (Rabi-like oscillations). These vanishing oscillations can be considered as the topological state migration from site to site, which was investigated, e.g., along the Majorana wire [47] after the quench. In our case this effect appear between two sites from different chains (fast oscillations). There are also visible long-period oscillations which are related to the zero-energy state migration along the chain and depend on the energy gap and the sideband energies. These oscillations last relatively long in time, Fig. 8, bottom panels, thus, it makes possible to detect these induced topological states in double-chain structures.

It is also interesting to analyze the SSH_0-SSH_1 system for a smaller change in the chain-chain coupling parameter V_x such that after the change the system still remains in the same topological phase. Surprisingly small, but a sudden change leads to unexpected results. In Fig. 10 we show LDOS dynamics at the first two sites of the SSH_0 and SSH_1 chains for a sudden quench at $t = 10$, and for $V_x = 3$ (thus, for $t > 10$ the system is in the nontrivial phase, cf. the energy spectrum in Fig. 7, bottom panel). In this case the edge midgap state (left upper panel) vanishes for a short period of time just after the quench. During this time zero-energy states appear at the neighboring sites. It is important that through these sites the SSH_1 topological state is partially transferred to the SSH_0

trivial chain (right bottom panel). For a longer time there are two midgap states in the system: (i) at the edge site in SSH_1 and (ii) at the second site in SSH_0. The intensity of the SSH_1 topological state decreases in comparison with its value before the quench (from a high value represented by a yellowlike color to the lower one—green color) because it leaks to the trivial SSH_0 chain. It is also worth noting that the electron occupancies of all sites in both chains do not change in time during this quench as the system is fully symmetrical.

To conclude, we have found that rapid change in V_x in the coupled SSH_0-SSH_1 system induces topological states in the trivial chain. As a main result we have observed that the SSH topological state can be partially transferred inside the system and exist simultaneously at different sites. It seems reasonable as for the coupled chains the unit cell is not longer the two-site primitive cell (as in the usual SSH chain) but is a four-site cell composed of two sites from the SSH_0 and two sites from the SSH_1 chains. Thus, the topological state of the coupled chains is still present at the end cell and can leak inside the cell.

C. Coulomb repulsion between atomic chains

Electron charge in a finite-length atomic chain can be distributed uniformly along the chain or can form charge waves called the Friedel oscillations [8,52]. These oscillations are the consequence of asymmetry of the spectral density functions at each site with respect to the Fermi energy. Note that charge oscillations are strongly suppressed in topological chains due to the energy gap in such systems. However, for a double-chain structure the charge waves along a given chain can be reproduced in the second one (in the same phase or in antiphase oscillations) in the presence of the Coulomb repulsion, but it is doubtful if these oscillations can appear in topological chains.

To answer this question in Fig. 11 we analyze the occupancies along two coupled chains (upper panel) obtained for $t \to \infty$ and $U^C = 0$ (thin curves) as well as in the presence of electron-electron repulsion $U^C = 5$ between both chains (thick curves). The charge waves in the normal chain at the substrate satisfy the condition for the period of three sites [52] ($\varepsilon_i = -V,\ U^C = 0$)—upper panel, thin broken green curve. In the vicinity of this chain there is a nontrivial topological chain SSH_1 with half-occupied sites (red solid line) and topological edge states. As one can see for nonzero U^C (thick lines) electrons in both chains repeal each other which leads, in general, to decreasing in the occupations in the normal and in the topological chains. However, charge oscillations in the normal chain are still observed, and they induce the Friedel oscillations along the topological chain. This effect is surprising and important for the studies of topological materials as there is an energy gap at the Fermi level in the SSH_1 chain. Note that high occupancy values in the normal chain stronger reduce charge values in the topological chain at the corresponding sites leading to the antiphase oscillations in this chain. It is also interesting that electron occupancy at the first site in the topological chain more rapidly decreases in comparison with the other site occupancies. It is a consequence of nontrivial midgap state at this site which in the presence of electron-electron repulsion is renormalized by the value of $U^C n_{1(\mathrm{nor})}$, where $n_{1(\mathrm{nor})}$ is the charge occupancy at the first site in the normal chain. Thus, even for small U^C the spectral density function is shifted towards higher energies and the electron occupancy at the first site drastically decreases whereas at other sites in the chain the changes are smaller due to the energy gap at the Fermi level.

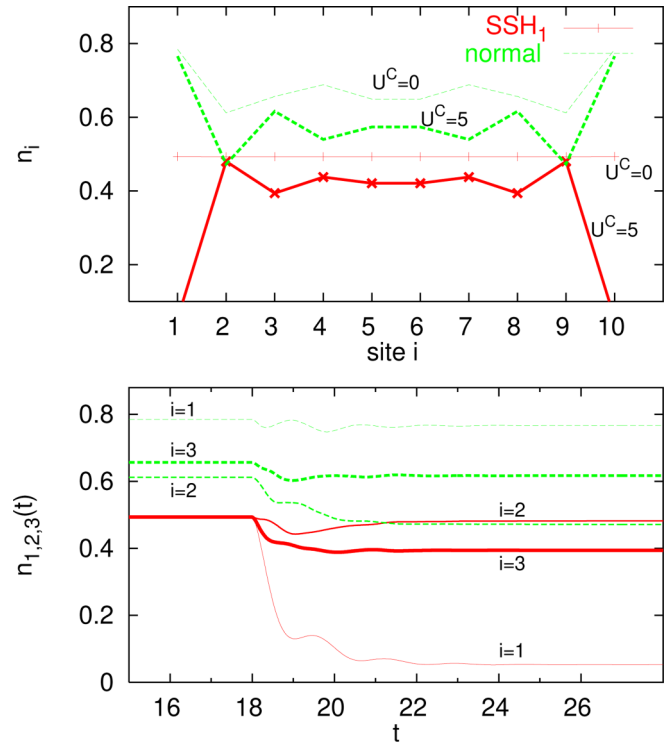

FIG. 11. Electron occupancies along the normal chain (broken green curves) and along the SSH_1 chain (solid red curves) of the length $N = 10$ for $U^C = 0$ (thin curves) and $U^C = 5$ (thick curves)—upper panel. The bottom panel shows time-dependent occupancies at $i = 1$–3 sites in both chains for a sudden change of the Coulomb repulsion $U^C = 0$ for $t < 18$ and $U^C = 5$ for $t \geqslant 18$. The other parameters are $V = 4,\ W = 1,\ \varepsilon_i = 0$ (topological chain) and $V,\ W = 4,\ \varepsilon_i = -V$ (normal chain). The lines in the upper panel are plotted for better visualization.

It is also interesting to analyze time evolution of the charge waves which are induced in the coupled chains of different topology. In Fig. 11, bottom panel, we show the occupancies at three sites of the normal chain (green broken curves) and the SSH_1 chain (red solid curves) for a sudden change in the Coulomb repulsion at $t = 18$ ($U^C = 5$). Before the Coulomb quench the occupancies are time independent and their values correspond to the steady case for $U^C = 0$. Also for $t \to \infty$ the electron occupancies reach their stationary values, the same as for $U^C = 5$ in the upper panel (thick curves). Just after the perturbation all occupancies change, and the time evolution of n_i shows vanishing oscillations. The period of these oscillations depends on the Coulomb repulsion and equals $T = \frac{2\pi}{U^C n_i}$ (which in our case is $T \simeq 1.6$). Thus, from the knowledge of time-dependent charge oscillations one can estimate the strength of the Coulomb interaction between the sites. It is worth noting that although the occupancies in general decrease in the presence of U^C, it is possible to inverse the occupancies between the neighboring sites in both chains and,

e.g., at the second sites $i = 2$ for $U^C = 0$ the charge at the normal chain is larger that in the SSH chain, but for nonzero U^C the opposite relation is satisfied. This process can lead to the electron localization in topological chains due to the Coulomb repulsion.

IV. CONCLUSIONS

We have studied nonequilibrium electrical properties of 1D topological chains and coupled chains on a surface focusing on the energy-dependent spectral density function. For a single chain we have analyzed the transition process from the normal chain to the SSH nontrivial chain where the midgap edge state appears. It turns out that the timescale needed to build this state strongly depends on the surface and for the insulating substrate the system reaches its equilibrium state after hundreds units of time from the quench. Moreover, we have found that the edge state is formed dynamically from the intersidebands of the normal chain (in the first stage after the quench) and then next sidebands support this state after some further period of time. Thus, the midgap state does not appear immediately after the quench and is formed simultaneously with the bulk energy gap. We have also analyzed topological chain which suddenly breaks. In this case the midgap topological state as well as the local DOS at all sites do not change in time except for two sites which comprise new edges of two shorter chains. At these sites, which are characterized by the energy gap, new midgap states are built adiabatically in time from the LDOS sidebands.

We have also considered coupled atomic chains being in the same or in different topological phases (SSH_0 or SSH_1) and studied the time response of the spectral density functions on abruptly or adiabatically changing of the chain-chain couplings V_x. For the SSH_0-SSH_0 geometry the energy gap can be closed (for small V_x) or is still present in the system (for larger V_x), but the midgap topological state does not appear. It is important that for the SSH_1-SSH_1 system the midgap zero-energy state splits adiabatically into two sidebands for small V_x or vanishes for larger V_x—in the last case the energy gap is open in the system. The most interesting case we have observed for different phases of the coupled chains SSH_0-SSH_1. We have found that for larger values of V_x the system changes its phase (from nontrivial to the trivial one) and the midgap topological state vanishes. However, for the adiabatical change in V_x the topological SSH_1 state partially leaks to the trivial SSH_0 chain, and both midgap states exist simultaneously at two different sites. For abruptly changed V_x the topological as well as the induced topological states vanish in time with damping oscillations. These novel conclusions have been obtained from the detail analysis of the full space- and time-dependent LDOS, supported by the quasienergy spectra, which give us a wider perspective on the midgap topological states.

We have also investigated the electron correlation effects between the coupled chains and the induced Friedel oscillations along the SSH chain were found in the vicinity of the normal chain with standard charge waves. The induced out-of-phase Friedel oscillations in topological structures stands for a crucial point of the paper. These oscillations with very low electron occupancy at both end sites can be the essential feature of 1D topology in potential STM experiments.

ACKNOWLEDGMENTS

This work was partially supported by National Science Centre, Poland, under Grant No. 2018/31/B/ST3/02370.

APPENDIX A: EVOLUTION OPERATOR CALCULATIONS

Here we give some details on the charge occupancy and the current obtained within the evolution operator method [49,50]. To derive the time-dependent occupations at a given site $n_i(t)$, one has to find the expectation value of the total particle number operator $\hat{n}_{all}$, taken for the time-dependent state vector related with this site $|\alpha_i\rangle$,

$$n_i(t) = \langle \alpha_i(t)|\, \hat{n}_{all}\, |\alpha_i(t)\rangle\,. \tag{A1}$$

The total particle number of the system can be written as a sum over all electron states $\hat{n}_{all} = \sum_j \hat{n}_j + \sum_{\vec{k},j} \hat{n}_{\vec{k}j}$ and the unitary evolution operator describes time transformation of the state vector from its initial state $|\alpha_i(t_0)\rangle$ such that: $|\alpha_i(t)\rangle = U(t,t_0)\,|\alpha_i(t_0)\rangle$. Now the ith site occupancy can be written in the following form:

$$n_i(t) = \langle \alpha_i(t_0)|\, U^\dagger(t,t_0)|\sum_j \hat{n}_j + \sum_{\vec{k},j} \hat{n}_{\vec{k}j}|U(t,t_0)\,|\alpha_i(t_0)\rangle\,. \tag{A2}$$

Let us consider the first sum in the above equation with $\hat{n}_j$ operators. Using the unit operator for this system which contains all single-particle states at the initial time $\mathbb{1} = \sum_\alpha |\alpha(t_0)\rangle\,\langle\alpha(t_0)|$, one can obtain the formula,

$$\begin{aligned}
&\sum_j \langle \alpha_i(t_0)|\, U^\dagger(t,t_0)|\hat{n}_j|U(t,t_0)\,|\alpha_i(t_0)\rangle \\
&\quad= \sum_j \langle \alpha_i(t_0)|\, U^\dagger(t,t_0)|\mathbb{1}|\hat{n}_j|\mathbb{1}|U(t,t_0)\,|\alpha_i(t_0)\rangle \\
&\quad= \sum_j \sum_\alpha \sum_{\alpha'} \langle \alpha_i(t_0)|\, U^\dagger(t,t_0)\,|\alpha(t_0)\rangle\, \underbrace{\langle\alpha(t_0)|\,\hat{n}_j\,|\alpha'(t_0)\rangle}_{\delta_{\alpha,j}\delta_{\alpha',j}n_j(t_0)} \\
&\qquad\times \langle\alpha'(t_0)|\,U(t,t_0)\,|\alpha_i(t_0)\rangle = \sum_j n_j(t_0)|U_{i,j}(t,t_0)|^2,
\end{aligned} \tag{A3}$$

which stands for the first term of Eq. (2). The second term in Eq. (A2) includes the wave-vector summation $\sum_{\vec{k}j} \langle \alpha_i(t_0)|\, U^\dagger(t,t_0)|\hat{n}_{\vec{k}j}|U(t,t_0)\,|\alpha_i(t_0)\rangle$ and using similar calculations as above one finally obtains the second term in Eq. (2). The electron occupancy of the electrode state $\vec{k}_1$, needed for the current calculations, Eq. (3), can be obtained from the following relation [it can be derived in the same way as Eq. (A3)]:

$$n_{\vec{k}_1}(t) = \sum_{j=1}^{M} n_j(t_0)|U_{\vec{k}_1,j}(t,t_0)|^2 + \sum_{j,\vec{k}_j} n_{\vec{k}_j}(t_0)|U_{\vec{k}_1,\vec{k}_j}(t,t_0)|^2. \tag{A4}$$

Thus, for the initial occupations $n_j(t_0) = 0$, the current flowing, e.g., through the first chain site, Eq. (3), is expressed by the formula,

$$j_1(t) = -e\frac{d}{dt}\sum_{\vec{k}_1}\sum_{j,\vec{k}_j} n_{\vec{k}_j}(t_0)|U_{\vec{k}_1,\vec{k}_j}(t,t_0)|^2$$
$$= \sum_{\vec{k}_1}\sum_{j,\vec{k}_j} 2n_{\vec{k}_j}(t_0)\mathrm{Re}\left(U^*_{\vec{k}_1,\vec{k}_j}(t,t_0)\frac{d}{dt}U_{\vec{k}_1,\vec{k}_j}(t,t_0)\right). \tag{A5}$$

To find the equation for the evolution operator $U_{\alpha,\beta}(t)$ one can use Eq. (4), which can be written as follows: $i\frac{\partial}{\partial t}U_{\alpha,\beta}(t) = \langle\alpha|\,\hat{V}(t)U(t)\,|\beta\rangle$. On the right-hand side we use the unity operator and obtain the coupled set of differential equations,

$$i\frac{\partial U_{\alpha,\beta}(t)}{\partial t} = \langle\alpha|\,\hat{V}(t)|\mathbb{1}|U(t)\,|\beta\rangle$$
$$= \sum_{j'}\langle\alpha|\,\hat{V}(t)\,|j'\rangle\underbrace{\langle j'|\,U(t)\,|\beta\rangle}_{U_{j',\beta}(t,t_0)}$$
$$+ \sum_{j',\vec{k}}\langle\alpha|\,\hat{V}(t)\,|\vec{k}_{j'}\rangle\underbrace{\langle\vec{k}_{j'}|\,U(t)\,|\beta\rangle}_{U_{\vec{k}_{j'},\beta}(t,t_0)}. \tag{A6}$$

The terms with $\hat{V}(t)$ are obtained using the Hamiltonian and the relations below Eq. (4), and one can write

$$\langle\alpha|\,\hat{V}(t)\,|\beta\rangle = \langle\alpha|\,U_0(t,t_0)|V(t)|U_0^\dagger(t,t_0)\,|\beta\rangle$$
$$= \langle\alpha|\,U_0(t,t_0)|\mathbb{1}|V(t)|\mathbb{1}|U_0^\dagger(t,t_0)\,|\beta\rangle$$
$$= (U_0)_{\alpha,\alpha}(t,t_0)(V(t))_{\alpha,\beta}(U_0^\dagger)_{\beta,\beta}(t,t_0), \tag{A7}$$

where, e.g., $(U_0)_{\alpha,\alpha}(t,t_0) = \exp\left(i\int_0^t dt'\,\langle\alpha|\,H_0(t')\,|\alpha\rangle\right)$. In the same way one can write the differential equations for other evolution operator matrix elements, such as for $U_{\vec{k}_{j'},\beta}(t,t_0)$ and insert their formal solutions into Eq. (A6) which finally gives the integodifferential Volterra equation of the second kind, Eq. (5).

APPENDIX B: LAPLACE TRANSFORM CALCULATIONS

In this Appendix we show some technical aspects for the calculation of Eq. (8) for $U_{i,\vec{k}_j}(t)$ matrix elements. We start from the differential equation, Eq. (5), written for the regular chain of the same sites with vanishing Coulomb interactions and within the wideband approximation, i.e.,

$$i\frac{\partial U_{i,\vec{k}_j}(t)}{\partial t} = \sum_{i'}V_{ii'}U_{i',\vec{k}_j}(t) - V_{i,\vec{k}_j}e^{i(\varepsilon_0-\varepsilon_{\vec{k}_j})t} - i\frac{\Gamma_i}{2}U_{i,\vec{k}_j}(t). \tag{B1}$$

Now we use the Laplace transform technique for this equation, $F_{ij}(s) \equiv \mathcal{L}[U_{i,\vec{k}_j}(t)] = \int_0^{+\infty}U_{i,\vec{k}_j}(t)e^{-st}dt$, and obtain the following set of linear recursive equations on $F_{ij}(s)$ elements,

$$\left(s+\frac{\Gamma_i}{2}\right)F_{ij}(s) + iV_{i,i+1}F_{i+1,j}(s) + iV_{i,i-1}F_{i-1,j}(s)$$
$$= \frac{-iV_{i,\vec{k}_j}}{s-i(\varepsilon_0-\varepsilon_{\vec{k}_j})}\delta_{ij}. \tag{B2}$$

The formal solution of these Laplace transform functions can be written as

$$F_{ij}(s) = \frac{-iV_{i,\vec{k}_j}}{s-i(\varepsilon_0-\varepsilon_{\vec{k}_j})}A^{-1}_{ij}, \tag{B3}$$

where $A_{ij} = (s+\frac{\Gamma_i}{2})\delta_{ij} + iV_{ij}(\delta_{i+1,j}+\delta_{i,j+1})$ is the tridiagonal matrix ($N\times N$ dimension, A^N) for which the determinant can be expressed by the Chebyshev polynomials of the second kind. For the same couplings between sites $V_{ij} = V$ and $\Gamma_i = \Gamma$, the Laplace transform elements take the following form (e.g., for $i = 1$):

$$F_{1j}(s) = \frac{(-i)^jV^{j-1}V_{j,\vec{k}_j}}{s-i(\varepsilon_0-\varepsilon_{\vec{k}_j})}\frac{\det A^{N-j}}{\det A^N}, \tag{B4}$$

where $\det A^N = \prod_{j=1}^N(s+\frac{\Gamma}{2}+2iV\,\cos\frac{j\pi}{N+1})$. Now, to obtain the solutions in the time domain we have to calculate the inverse Laplace transforms: $U_{i,\vec{k}_j}(t) = \mathcal{L}^{-1}\{F_{ij}(s)\}$, which in our case can be performed analytically as the determinant of (B4) contains only the product terms of s variable. The final result is given by Eq. (8).

[1] M. Kopciuszyński, P. Dyniec, M. Krawiec, P. Łukasik, M. Jałochowski, and R. Zdyb, Pb nanoribbons on the si(553) surface, Phys. Rev. B **88**, 155431 (2013).

[2] J. N. Crain, J. L. McChesney, F. Zheng, M. C. Gallagher, P. C. Snijders, M. Bissen, C. Gundelach, S. C. Erwin, and F. J. Himpsel, Chains of gold atoms with tailored electronic states, Phys. Rev. B **69**, 125401 (2004).

[3] A. Baski, K. Saoud, and K. Jones, 1-d nanostructures grown on the si(5 5 12) surface, Appl. Surf. Sci. **182**, 216 (2001).

[4] M. Jałochowski, T. Kwapinski, P. Łukasik, P. Nita, and M. Kopciuszyński, Correlation between morphology, electron band structure, and resistivity of pb atomic chains on the si(553)-au surface, J. Phys.: Condens. Matter **28**, 284003 (2016).

[5] H. Ohnishi, Y. Kondo, and K. Takayanagi, Quantized conductance through individual rows of suspended gold atoms, Nature (London) **395**, 780 (1998).

[6] A. Yanson, G. Rubio-Bollinger, H. E. Brom, N. Agrait, and J. van Ruitenbeek, Formation and manipulation of a metallic wire of single gold atoms, Nature (London) **395**, 783 (1998).

[7] O. M. Auslaender, H. Steinberg, A. Yacoby, Y. Tserkovnyak, B. I. Halperin, K. W. Baldwin, L. N. Pfeiffer, and K. W. West, Spin-charge separation and localization in one dimension, Science **308**, 88 (2005).

[8] J. S. Shin, K.-D. Ryang, and H. W. Yeom, Finite-length charge-density waves on terminated atomic wires, Phys. Rev. B **85**, 073401 (2012).

[9] S. Nadj-Perge, I. K. Drozdov, J. Li, H. Chen, S. Jeon, J. Seo, A. H. MacDonald, B. A. Bernevig, and A. Yazdani, Observation of majorana fermions in ferromagnetic atomic chains on a superconductor, Science **346**, 602 (2014).

[10] R. Pawlak, M. Kisiel, J. Klinovaja, T. Meier, S. Kawai, T. Glatzel, D. Loss, and E. Meyer, Probing atomic structure and majorana wavefunctions in mono-atomic fe chains on superconducting pb surface, npj Quantum Inf. **2**, 16035 (2016).

[11] L. Li, Z. Xu, and S. Chen, Topological phases of generalized Su-Schrieffer-Heeger models, Phys. Rev. B **89**, 085111 (2014).

[12] L. Li, C. Yang, and S. Chen, Winding numbers of phase transition points for one-dimensional topological systems, Europhys. Lett. **112**, 10004 (2015).

[13] M. Benito, M. Niklas, G. Platero, and S. Kohler, Edge-state blockade of transport in quantum dot arrays, Phys. Rev. B **93**, 115432 (2016).

[14] V. Dal Lago, M. Atala, and L. E. F. Foa Torres, Floquet topological transitions in a driven one-dimensional topological insulator, Phys. Rev. A **92**, 023624 (2015).

[15] W. P. Su, J. R. Schrieffer, and A. J. Heeger, Solitons in Polyacetylene, Phys. Rev. Lett. **42**, 1698 (1979).

[16] R. Drost, T. Ojanen, A. Harju, and P. Liljeroth, Topological states in engineered atomic lattices, Nat. Phys. **13**, 668 (2017).

[17] J. K. Asboth, L. Oroszlany, and A. Palyi, *A Short Course on Topological Insulators* (Springer, Cham, Switzerland, 2016).

[18] M. Kurzyna and T. Kwapiński, Non-local electron transport through normal and topological ladder-like atomic systems, J. Appl. Phys. **123**, 194301 (2018).

[19] D. Xie, W. Gou, T. Xiao, B. Gadway, and B. Yan, Topological characterizations of an extended Su-Schrieffer-Heeger model, npj Quantum Inf. **5**, 55 (2019).

[20] V. M. Martinez Alvarez and M. D. Coutinho-Filho, Edge states in trimer lattices, Phys. Rev. A **99**, 013833 (2019).

[21] B. Pérez-González, M. Bello, Á. Gómez-León, and G. Platero, Interplay between long-range hopping and disorder in topological systems, Phys. Rev. B **99**, 035146 (2019).

[22] B. Pérez-González, M. Bello, Álvaro Gómez-León, and G. Platero, SSH model with long-range hoppings: topology, driving and disorder, arXiv:1802.03973.

[23] B.-H. Chen and D.-W. Chiou, An elementary rigorous proof of bulk-boundary correspondence in the generalized Su-Schrieffer-Heeger model, Phys. Lett. A **384**, 126168 (2020).

[24] X.-L. Lü and H. Xie, Topological phases and pumps in the Su-Schrieffer-Heeger model periodically modulated in time, J. Phys.: Condens. Matter **31**, 495401 (2019).

[25] J. H. Kang, J. H. Han, and Y. Shin, Creutz ladder in a resonantly shaken 1d optical lattice, New J. Phys. **22**, 013023 (2020).

[26] N. Sun and L.-K. Lim, Quantum charge pumps with topological phases in a creutz ladder, Phys. Rev. B **96**, 035139 (2017).

[27] J. Zurita, C. E. Creffield, and G. Platero, Topology and interactions in the photonic creutz and creutz-hubbard ladders, Adv. Quantum Technol. **3**, 1900105 (2019).

[28] K. Pöyhönen, A. Weststrom, J. Röntynen, and T. Ojanen, Majorana states in helical shiba chains and ladders, Phys. Rev. B **89**, 115109 (2014).

[29] D. Obana, F. Liu, and K. Wakabayashi, Topological edge states in the Su-Schrieffer-Heeger model, Phys. Rev. B **100**, 075437 (2019).

[30] J. Arkinstall, M. H. Teimourpour, L. Feng, R. El-Ganainy, and H. Schomerus, Topological tight-binding models from nontrivial square roots, Phys. Rev. B **95**, 165109 (2017).

[31] A. Gómez-León and G. Platero, Floquet-Bloch Theory and Topology in Periodically Driven Lattices, Phys. Rev. Lett. **110**, 200403 (2013).

[32] O. Balabanov and H. Johannesson, Robustness of symmetry-protected topological states against time-periodic perturbations, Phys. Rev. B **96**, 035149 (2017).

[33] T. Kitagawa, E. Berg, M. Rudner, and E. Demler, Topological characterization of periodically driven quantum systems, Phys. Rev. B **82**, 235114 (2010).

[34] T. Ochiai, Su-Schrieffer-Heeger-type Floquet network, arXiv:1811.11984.

[35] C. Jürß and D. Bauer, High-harmonic generation in Su-Schrieffer-Heeger chains, Phys. Rev. B **99**, 195428 (2019).

[36] M. Bello, C. E. Creffield, and G. Platero, Long-range doublon transfer in a dimer chain induced by topology and ac fields, Sci. Rep. **6**, 22562 (2016).

[37] J. Huneke, G. Platero, and S. Kohler, Steady-State Coherent Transfer by Adiabatic Passage, Phys. Rev. Lett. **110**, 036802 (2013).

[38] N. H. Le, A. J. Fisher, N. J. Curson, and E. Ginossar, Topological phases of a dimerized fermi–hubbard model for semiconductor nano-lattices, npj Quantum Inf. **6**, 24 (2020).

[39] T. Hensgens, T. Fujita, L. Janssen, X. Li, C. J. Van Diepen, C. Reichl, W. Wegscheider, S. Das Sarma, and L. M. K. Vandersypen, Quantum simulation of a fermi–hubbard model using a semiconductor quantum dot array, Nature (London) **548**, 70 (2017).

[40] F. A. Zwanenburg, A. S. Dzurak, A. Morello, M. Y. Simmons, L. C. L. Hollenberg, G. Klimeck, S. Rogge, S. N. Coppersmith, and M. A. Eriksson, Silicon quantum electronics, Rev. Mod. Phys. **85**, 961 (2013).

[41] E. J. Meier, F. A. An, and B. Gadway, Observation of the topological soliton state in the Su-Schrieffer-Heeger model, Nat. Commun. **7**, 13986 (2016).

[42] M. Parto, S. Wittek, H. Hodaei, G. Harari, M. A. Bandres, J. Ren, M. C. Rechtsman, M. Segev, D. N. Christodoulides, and M. Khajavikhan, Edge-Mode Lasing in 1d Topological Active Arrays, Phys. Rev. Lett. **120**, 113901 (2018).

[43] E. Taranko, M. Wiertel, and R. Taranko, Transient electron transport properties of multiple quantum dots systems, J. Appl. Phys. **111**, 023711 (2012).

[44] X. Li, Y. Meng, X. Wu, S. Yan, Y. Huang, S. Wang, and W. Wen, Su-Schrieffer-Heeger model inspired acoustic interface states and edge states, Appl. Phys. Lett. **113**, 203501 (2018).

[45] C.-C. Chien, K. A. Velizhanin, Y. Dubi, B. R. Ilic, and M. Zwolak, Topological quantization of energy transport in micromechanical and nanomechanical lattices, Phys. Rev. B **97**, 125425 (2018).

[46] A. Rajak and A. Dutta, Survival probability of an edge majorana in a one-dimensional *p*-wave superconducting chain under sudden quenching of parameters, Phys. Rev. E **89**, 042125 (2014).

[47] P. D. Sacramento, Fate of majorana fermions and chern numbers after a quantum quench, Phys. Rev. E **90**, 032138 (2014).

[48] C. H. Lee and J. C. W. Song, Quenched topological boundary modes can persist in a trivial system, arXiv:2002.11726.

[49] T. B. Grimley and K. L. Sebastian, Electron transfer in the reflection of atoms from metal surfaces, Surf. Sci. **124**, 305 (1983).

[50] T. Kwapiński, Conductance oscillations and charge waves in zigzag shaped quantum wires, J. Phys.: Condens. Matter **22**, 295303 (2010).

[51] T. Kwapiński, Conductance oscillations of a metallic quantum wire, J. Phys.: Condens. Matter **17**, 5849 (2005).

[52] T. Kwapiński, Charge fluctuations in a perfect and disturbed quantum wire, J. Phys.: Condens. Matter **18**, 7313 (2006).